New insights into the origin of two contrasting Himalayan granite belts

T. Mark Harrison
Oscar M. Lovera
Marty Grove

Department of Earth and Space Sciences and Institute of Geophysics and Planetary Physics, University of California, Los Angeles, California 90095

ABSTRACT

The two parallel belts of Miocene granite that extend along much of the Himalaya differ in age, petrogenesis, and emplacement style. We suggest that their origin is linked to shear heating on a continuously active decollement that cuts through previously metamorphosed Indian supracrustal rocks that were transformed into basement during the initial stages of the Indian-Asian collision. Numerical simulations assuming a shear stress of 30 MPa indicate that initiation of slip on the Himalayan thrust at 24 Ma could trigger discontinuous melting reactions leading to formation of the High Himalayan granite chain from 24 to 20 Ma and the North Himalayan belt from 18 to 12 Ma. This model result agrees well with observation as do model predictions regarding emplacement style and location.

INTRODUCTION

A long-standing puzzle in Himalayan geology is the origin of the two parallel granite belts that span much of the mountain range (Fig. 1).[1] The High Himalayan leucogranites form a discontinuous chain of sills and dikes that are exposed adjacent to the South Tibetan detachment, which separates Indian gneisses of the Tibetan slab from lower-grade Tethyan shelf deposits in the hanging wall (Fig. 1). The plutons of the Zanskar, Garhwal, Manaslu, and Everest-Makalu regions, which comprise ~75% of the ~8000 km^2 of leucogranite exposed along the crest of the High Himalaya (Le Fort et al., 1987), appear to have been largely emplaced between 24 and 19 Ma (see Fig. 1 caption) at temperatures of ~700 °C (Montel, 1993). About half of the remaining 25% are undated plutons from central Bhutan, and <5% yield ages of ca. 17 Ma (e.g., Searle et al., 1997).

The North Himalayan granite belt runs parallel to, and ~100 km to the north of, the High Himalaya. It is composed of ~16 elliptical-shaped plutons totaling ~4000 km^2 in area that generally intrude into Tethyan metasedimentary rocks (Le Fort, 1986). They differ from the High Himalayan leucogranites in their emplacement style (Fig. 1), younger ages (17–10 Ma), and higher melting temperatures (>750 °C) suggested by noneutectic compositions and high light rare earth contents coupled with low monazite inheritance (Debon et al., 1986; Schärer et al., 1986; Montel, 1993).

Models for the origin of the High Himalayan leucogranites have focused on their relationship with the South Tibetan detachment and the Main Central thrust, which separates the Tibetan slab from the lower-grade Midlands formations and their spatial association with the inverted pattern of metamorphism developed below the thrust (Fig. 1). These models have investigated the effects of fluid infiltration, decompression melting, mantle delamination, high radioactivity, and shear heating (see summary in Harrison et al., 1997). The relative youth of the North Himalayan granites has been ascribed to a low rate of fluid infiltration (Le Fort, 1986) and thermal refraction (Pinet and Jaupart, 1987).

Models seeking a causal relationship between Tibetan slab anatexis and inverted metamorphism have had to invoke an extraordinary source of heat that permits melting in the hanging wall of the Main Central thrust while subduction of India refrigerates the system. Recent investigations in the central Himalaya indicate that recrystallization of the Main Central thrust footwall is a recent phenomenon (i.e., 8–4 Ma) and thus not temporally related to Tibetan slab anatexis (Harrison et al., 1997). Recognition of this timing disparity obviates the need to restrict anatexis to the Main Central thrust ramp (e.g., Molnar and England, 1990). This result, together with recent studies indicating that the master decollement dips shallowly to the north (e.g., Brown et al., 1996), suggests that the origin of the two granite belts be revisited. We propose an alternative model that ascribes the spatial and temporal variations of granite emplacement to continuous slip on the shallowly dipping decollement.

GEOLOGIC AND PETROLOGIC FRAMEWORK

The ~1000 km of shortening between the Indian Shield and southern Tibet since collision began at 55 Ma (Chen et al., 1993; Patzelt et al., 1996) appears to have been largely taken up by the Himalayan (Le Fort, 1996) and Tethyan

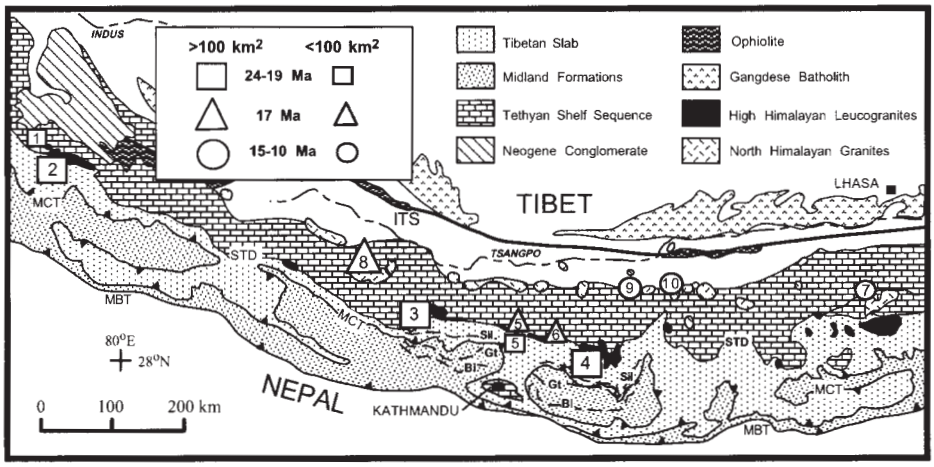

Figure 1. Geologic sketch map of Himalaya showing location of High Himalayan and North Himalayan belts. MCT—Main Central thrust, MBT—Main Boundary thrust, STD—Southern Tibetan detachment, ITS—Indus Tsangpo suture. Plutons ≥100 km^2 are enumerated in large type and those <100 km^2 in smaller type. Different shapes represent the three emplacement intervals shown. Sources of U-Th-Pb monazite ages are (1) Gangotri (22.4 ± 0.5 Ma, this study, see footnote 1), (2) Shivling (21.9 ± 0.5 Ma; this study), (3) Manaslu (22.4 ± 0.5 and 19 ± 1; Harrison et al., 1995; Coleman and Parrish, 1995), (4) Everest-Makalu (23 ± 1 Ma; Schärer, 1984; Harrison et al., 1995), (5) Shisha Pangma (20–17 Ma; Searle et al., 1997), (6) Nyalam (16.8 ± 0.6 Ma; Schärer et al., 1986), (7) Gonto-La (12.5 ± 0.5 Ma; Edwards and Harrison, 1997); (8) Mugu (17.6 ± 0.3 Ma; this study, see footnote 1), (9) Lhagoi Kangri (15.1 ± 0.5 Ma; Schärer et al., 1986), (10) Maja (9.5 ± 0.5; Schärer et al., 1986), and (11) Zanskar (not shown) (20.0 ± 0.5 Ma; Noble and Searle, 1995).

[1]GSA Data Repository item 9749 (Th-Pb monazite results for Gangotri, Shivling, and Mugu granites) is available on request from Documents Secretary, GSA, P.O. Box 9140, Boulder, CO 80301. E-mail: editing@geosociety.org.

Data Repository item 9749 contains additional material related to this article.

(Ratschbacher et al., 1994) thrust systems. Prior to collision, the northern Indian margin was composed of a thinned cratonic wedge over which was draped both Proterozoic clastic deposits and the Cambrian-Eocene Tethyan shelf sequence (Le Fort, 1996). The protoliths of the Midlands Formations and Tibetan slab are interpreted, respectively, to be Middle and Late Proterozoic clastic rocks (Parrish and Hodges, 1996). Our starting point is to assume that immediately prior to collision the northern Indian margin resembled Figure 2A. During the initial eo-Himalayan (ca. 55–35 Ma) stage of collision (Le Fort, 1996), the Tibetan slab protolith underwent high-grade recrystallization and anatexis (e.g., Hodges et al., 1994, 1996; Coleman and Parrish, 1995; Parrish and Hodges, 1996; Edwards and Harrison, 1997).

Although the nature of eo-Himalayan crustal thickening is poorly known, we assume it to have occurred via pure shear (Fig. 2B). Metamorphism and anatexis in Tibetan slab protolith would produce a stratified paragenetic sequence in which dehydration and partial melting reactions caused grade to increase regularly with depth (Fig. 2B). In our model, we have represented the largely arkosic to pelitic rocks within the hanging wall of the Main Central thrust by the model assemblage muscovite (mus) + biotite (bio) + quartz (qtz) ± kyanite/sillimanite (als) ± K-feldspar (ksp). Partial melting of the source region can be characterized by two discontinuous reactions (Thompson, 1982; Fig. 2B): a lower-temperature "wet" melting in the presence of an aqueous fluid (reaction A), and a higher-temperature, "dry" melting reaction (reaction B). Using such a framework, we represent the eo-Himalayan paragenetic sequence in the hanging wall (Fig. 2B) as increasing in grade with depth from mus + qtz + bio ± als ± ksp (region X) to mus + qtz + bio ± als (region Y) as a result of reaction A and ultimately to bio + qtz ± als (region Z) due to reaction B. We further assume that Indian cratonic rocks beneath the Himalayan decollement are at granulite facies (i.e., dehydration melting is not permitted in the footwall). Because eo-Himalayan granitoids are known (e.g., Hodges et al., 1996), but apparently not abundant, silicate melts produced during this phase of shortening may have largely been restricted to migmatitic sequences that were susceptible to remelting during Miocene thrusting. We assume that the peak thermal structure resulting from the processes described above had not significantly decayed when the Main Central thrust began to slip.

For the scenario outlined above, reaction A proceeds at ~680 °C (= T_A) under graphite-saturated conditions (Ohmoto and Kerrick, 1977), while reaction B occurs at ~780 °C (= T_B) under fluid-absent conditions (Vielzeuf and Holloway, 1988). However, other possibilities exist. For example, if prior melt extraction had reduced H_2O activities below the values required by graphite saturation such that reaction A could not occur, the High Himalayan leucogranites may have instead resulted from muscovite dehydration melting (reaction B). In that case, the North Himalayan granites may have been produced by other, higher temperature reactions (e.g., biotite dehydration melting).

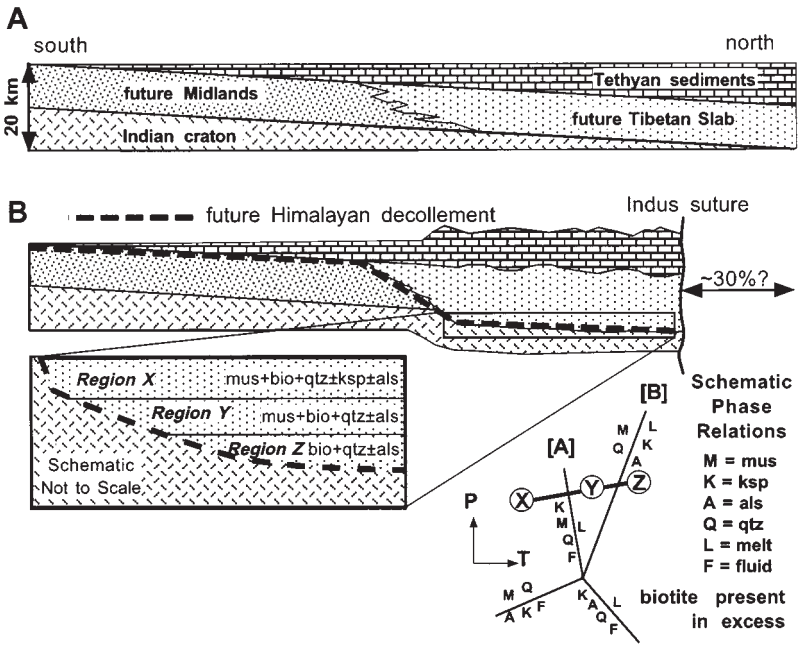

Figure 2. A: Possible distribution of Tethyan sediments and protoliths of Tibetan slab and Midlands formations with respect to Indian cratonic margin at ca. 55 Ma. B: During eo-Himalayan thickening at ca. 40 Ma, Tibetan slab protolith undergoes recrystallization and anatexis to produce mineral zonation shown in enlargement. Schematic petrogenetic grid illustrates model melting equilibria. Note that only region X preserves components required for minimum melting. Phase assemblage in region Y is produced from reaction A, whereas that in region Z results from reaction B. All melts produced during eo-Himalayan metamorphism are assumed to have been removed from regions Y and Z by ca. 40 Ma.

THERMAL MODEL

The thermal evolution of the thrust was simulated using a two-dimensional finite-difference model that employs flexural-bending deformation in both hanging wall and footwall (see Harrison et al., 1997). Zero-flux lateral boundaries were imposed and the basal heat flux was prescribed to yield an initial geotherm of 20 °C/km. We approximated the geometry of the ca. 24 Ma thrust system as a 30° ramp between 0 and 30 km depth, a 3° ramp between 30 and 35 km, followed by a horizontal segment (Fig. 3A). The shallowly dipping fault segment was simulated by linearly increasing temperature from left to right along the top boundary of the grid at a rate of 0.9 °C/km. Although we assume a linear 20 °C/km gradient for simplicity, the lower crustal geotherm for the more realistic case of depth-varying radioactivity is ~40% lower, corresponding in the model to a dip angle close to that presently observed (~9°; Brown et al., 1996).

We approximated shear heating within a 1-km-thick zone by the viscous dissipation produced by Couette flow between parallel walls assuming a constant shear stress (σ) of 30 MPa (cf. England and Molnar, 1993). Although higher values of σ are likely to be attained at the thrust toe and above the brittle-ductile transition, the predictions of our model are restricted to the thrust flat, and thus the value of σ we select need only be relevant to the basal decollement.

We simulated the thermal effects of melting due to reactions A and B by introducing a heat sink equal to 100% conversion of the dissipative energy into latent heat of fusion when melting temperatures were reached. An upper bound on the total melt production (M; i.e., column height) along unit length of the shear zone (Δt = 1 m.y.) is given by $M = (c_p/L)(\sigma V/K)(\kappa\Delta t)$ = 550 m (Turcotte and Schubert, 1982; see Table 1). This value is about two orders of magnitude higher

TABLE 1. MODEL PARAMETERS

Parameter	Definition
σ	shear stress = 30 MPa
V_h	hanging-wall velocity = 10 mm/yr
V_f	footwall velocity = −10 mm/yr
V	$\lvert V_h - V_f \rvert$ = 20 mm/yr
K	thermal conductivity = 2.5 W/(m·K)
κ	thermal diffusivity = 10^{-6} m^2/s
c_P	heat capacity = 1 kJ/(kg·K)
L	latent heat of fusion = 400 kJ/kg
Q_B	basal heat flux = 66 mW/m^2
T_A	temperature of reaction A = 680 °C
T_B	temperature of reaction B = 780 °C

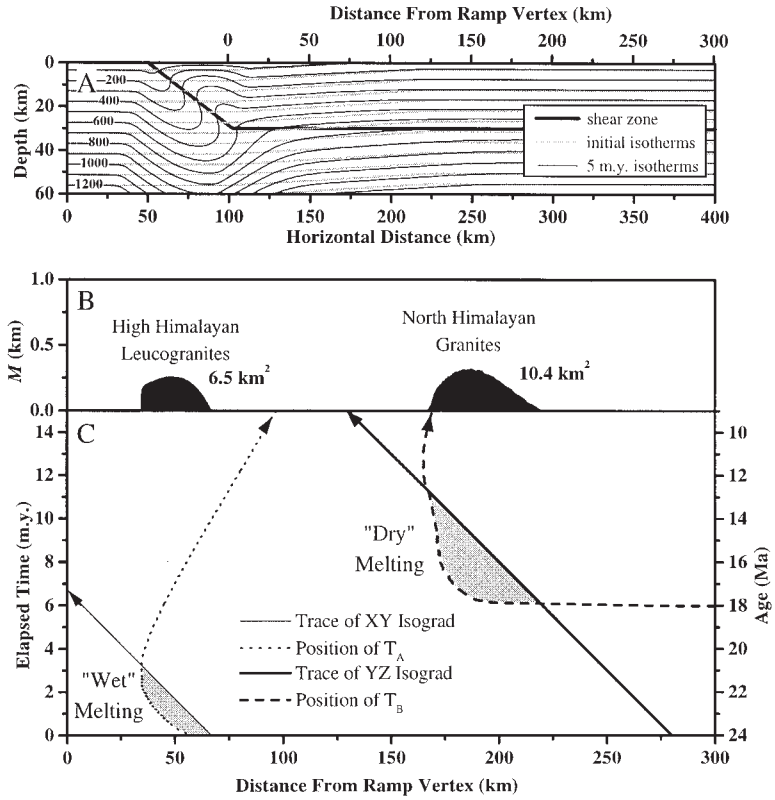

Figure 3. A: Representation of two-dimensional finite difference model. Shear zone location is shown by heavy line. Region of calculation was enclosed in a 400 km wide × 60 km deep grid with a resolution of 800 × 210. B: Melt production vs. distance from fault vertex. Two melting peaks correspond to melting reactions A and B discussed in the text. C: Plot shows positions of both the isograd boundaries and onset of melting along thrust for both reactions A and B as function of time. Overlap of these curves (indicated by shaded regions) indicates spatial and temporal conditions for which partial melting occurs. To form High Himalayan leucogranites, melting begins ~60 km from ramp at 24 Ma and terminates at 20 Ma at a distance of ~40 km from ramp. Melting to form the North Himalayan granites does not begin until 18 Ma and continues until 12 Ma.

than needed to explain the present ~3% exposure of Tertiary leucogranites in the Himalaya, assuming a pluton thickness of ~3 km (e.g., Le Fort, 1986, Searle et al., 1993).

RESULTS AND DISCUSSION

Our modeling results indicate that slip along a shallowly dipping fault within a metamorphically stratified crust can produce two horizontally separated granite belts through discontinuous partial melting reactions. The initial temperature (T_{ini}) distribution along the shear zone (Fig. 3A) primarily dictates where and when melting begins, as it is the difference between the T_{ini} and T_A or T_B at any point along the shear zone that determines the time required for the dissipative heating to raise T_{ini} to the melting temperature.

Applying the present-day (Bilham et al., 1997) slip rate (V) of 20 mm/yr to the period 24–10 Ma, the first phase of anatexis resulting from reaction A (T_A = 680 °C) begins almost immediately (i.e., 24 Ma; Fig. 3C) at a horizontal distance of ~60 km from the fault vertex (Fig. 3B). Figure 3C shows the positions of both the isograd boundaries and onset of melting along the thrust for reactions A and B as a function of time. The overlap of these curves (indicated by shaded regions) indicates the spatial and temporal conditions for which partial melting occurs. Progress of the two melting fronts is determined by the interplay between shear heating and diffusive heat loss. The refrigeration of the shear zone near the fault ramp, and the propagation of the melting front toward the ramp, ultimately causes melting to cease at t = 4 m.y. (i.e., 20 Ma; Fig. 3C). Note that melting due to reaction A no longer occurs at any location along the thrust because the necessary reactants occur only within region X. The second phase of melting begins when temperatures exceed T_B at t = 6 m.y. (i.e., 18 Ma; Fig. 3C) and continues until t = 12 m.y. (i.e., 12 Ma; Fig. 3C). Assuming that these viscous magmas preferentially remain in the middle crust, and that the observed ~3 km pluton thickness is characteristic, the total area of melt in our two-dimensional model (Fig. 3B) of 0.3% is broadly consistent with the 3% leucogranite currently exposed in the Himalaya.

The Main Central thrust ramp may have either been inactive during middle Miocene time, when slip occurred on both the Main Boundary and Renbu Zedong thrusts (Le Fort, 1996; Quidelleur et al., 1997), or not developed until the late Miocene. The first case would have little effect on our conclusions, since model predictions in that interval apply only to the continuously active decollement, and changes in the position of thrust ramps at the extreme ends of the model would not influence the thermal structure where North Himalayan granite production was occurring. In the second case, assuming that the Himalayan thrust was a single ramp with an average dip of ~9°, the model would underestimate the duration of melting in the High Himalayan leucogranite source region.

The model is sensitive to the choice of thrust geometry, magnitude of σV, initial position of isograd boundaries, and temperatures of the melting reactions. Note that the significant difference in time (~6 m.y.) between the onset of melting in the two belts dictates that the rocks along the horizontal segment of the fault are initially at a lower temperature than that needed to initiate melting by reaction B. Delaying melting by reaction B for 6 m.y. requires setting the initial temperature of the thrust flat to a value $T = T_B - [(\sigma V/K)(\kappa t/\pi)^{1/2}]$ (see Table 1) for t = 6 m.y. Numerical calculations indicate that displacement of the initial isograd boundaries to temperatures lower than T_A or T_B results in a decrease of melt production according to $M \propto e^{-\Delta T/6}$. Reducing σV by a factor of three leads to a 20-fold decrease in melt production.

A final consideration is whether a shear stress of 30 MPa is attainable in crustal rocks undergoing partial melting. Although the rheological properties of felsic rocks containing small amounts of melt (≤10%) at low strain rates are comparable to unmelted equivalents (Dell'Angelo and Tullis, 1988), experimental deformation studies of some "wet" crustal rocks suggest somewhat lower values of σ (Engelder, 1993). This apparent disparity is transcended if the high strain zone were maintained at the interface between Indian granulite and the dehydrated base of the Tibetan slab, as experimental results and paleopiezometric studies (Engelder, 1993) are consistent with a shear stress value of 30 MPa under relatively dry conditions. In this view, shear heating along the decollement raises temperatures sufficiently in the fertile, overlying rocks to induce anatexis. We conclude that our choice of 30 MPa as the characteristic shear stress along the decollement is not unreasonable and note that it is between 3 and 40 times lower than previously proposed for models of the thermal evolution of the Main Central thrust (e.g., England and Molnar, 1993).

SUMMARY

Although refrigeration due to underthrusting is important along a steeply dipping ramp, its effect is significantly diminished on the thrust flat. At locations distant from the ramp vertex, relatively low shear stresses (10–30 MPa) along a fault can

locally generate enough heat to produce anatexis. Model calculations indicate that two distinctive and spatially separated granite belts could be created by discontinuous melting reactions during continuous slip on a thrust surface that dips shallowly through a metamorphically stratified crust. The model makes several predictions that appear in accord with observation. (1) The ~100 km separation between the two model melting reactions (Fig. 3B) is similar to the distance between the granite belts (Fig. 1). Depending upon the position of magma emplacement (i.e., above the South Tibetan detachment), this spacing could approximate the distance separating the two belts. (2) Initiation of slip at 24 Ma predicts anatexis of the High Himalayan and North Himalayan belts at 24–20 Ma and 18–12 Ma, respectively; this agrees with the known ages of peak melt production of 24–19 and 17–10 Ma, respectively. (3) The volume of magma calculated from the model is broadly consistent with that inferred from the present outcrop pattern. (4) The highly viscous minimum melts produced by reaction A would likely be emplaced close to their source. Indeed, the High Himalayan leucogranites appear to be locally derived and emplaced syntectonically as sills and dikes (Le Fort, 1986; Searle et al., 1993). In contrast, the hotter and higher melt fraction magmas produced by reaction B are expected to be sufficiently buoyant and thermally energetic to ascend into the middle crust. The North Himalayan granites are generally emplaced into low grade Tethyan metasedimentary rocks and appear to have relatively higher melting temperatures. (5) The ramp-flat model (Fig. 3A) predicts that the Tibetan slab immediately above the present exposure of the Main Central thrust did not experience temperatures high enough to cause widespread melting. This last prediction is consistent with the observation that the protolith of the presently exposed High Himalayan leucogranites cannot be traced to sillimanite migmatites immediately above the Main Central thrust, which at many locations remain fertile for muscovite dehydration melting (e.g., Harris and Massey, 1994; Barbey et al., 1996).

ACKNOWLEDGMENTS

This research was support by a grant from the National Science Foundation. We greatly appreciate reviews by W. Hames, P. Le Fort, C. Manning, L. Ratschbacher, T. Rushmer, and F. Spear.

REFERENCES CITED

Barbey, P., Brouand, M., LeFort, P., and Pêcher, A., 1996, Granite-migmatite genetic link: The example of the Manaslu granite and Tibetan Slab migmatites in central Nepal: Lithos, v. 38, p. 63–79.

Bilham, R., Larson, K., Freymueller, J., and Project Idylhim members, 1997, GPS measurements of present-day convergence across the Nepal Himalaya: Nature, v. 386, p. 61–64.

Brown, L. D., Zhao, W., Nelson, K. D., Hauck, M., Alsdorf, D., Ross, A., Cogan, M., Clark, M., Liu, X., and Che, J., 1996, Bright spots, structure, and magmatism in southern Tibet from INDEPTH seismic reflection profiling: Science, v. 274, p. 1688–1691.

Chen, Y., Courtillot, V., Cogne, J. P., Besse, J., Yang, Z., and Enkin, R., 1993, The configuration of Asia prior to the collision of India: Cretaceous paleomagnetic constraints: Journal of Geophysical Research, v. 98, p. 21927–21941.

Coleman, M. E., and Parrish, R. R., 1995, Constraints on Miocene high-temperature deformation and anatexis within the Greater Himalaya from U-Pb geochronology: Eos (Transactions, American Geophysical Union), v. 76, p. F708.

Debon, F., Le Fort, P., Sheppard, S. M. F., and Sonet, J., 1986, The four plutonic belts of the Transhimalaya-Himalaya: A chemical, mineralogical, isotopic, and chronological synthesis along a Tibet-Nepal granite section, Journal of Petrology, v. 21, p. 219–250.

Dell'Angelo, L. N., and Tullis, J., 1988, Experimental deformation of partially molten granitic aggregates: Journal of Metamorphic Geology, v. 6, p. 495–515.

Edwards, M. A., and Harrison, T. M., 1997, When did the roof collapse? Late Miocene north-south extension in the high Himalaya revealed by Th-Pb monazite dating of the Khula Kangri granite: Geology, 25, 543–546.

Engelder, T., 1993, Stress regimes in the lithosphere: Princeton, New Jersey, Princeton University Press, 457 p.

England, P., and Molnar, P., 1993, The interpretation of inverted metamorphic isograds using simple physical calculations: Tectonics, v. 12, p. 145–157.

Harris, N., and Massey, J., 1994, Decompression and anatexis of Himalayan metapelites: Tectonics, v. 13, p. 1537–1546.

Harrison, T. M., McKeegan, K. D., and LeFort, P., 1995, Detection of inherited monazite in the Manaslu leucogranite by $^{208}Pb/^{232}Th$ ion microprobe dating: Crystallization age and tectonic significance: Earth and Planetary Science Letters, v. 133, p. 271–282.

Harrison, T. M., Ryerson, F. J., Le Fort, P., Yin, A., Lovera, O. M., and Catlos, E. J., 1997, A late Miocene-Pliocene origin for the Central Himalayan inverted metamorphism: Earth and Planetary Science Letters, v. 146, p. E1–E8.

Hodges, K. V., Parrish, R. R., and Searle M. P., 1996, Tectonic evolution of the central Annapurna Range, Nepalese Himalayas: Tectonics, v. 15, p. 1264–1291.

Hodges, K. V., Hames, W. E., Olszewski, W. J., Burchfiel, B. C., Royden, L. H., and Chen, Z., 1994, Thermobarometric and $^{40}Ar/^{39}Ar$ geochronologic constraints on Eohimalayan metamorphism in the Dinggy area, southern Tibet: Contributions to Mineralogy and Petrology, v. 117, p. 151–163.

Le Fort, P., 1986, Metamorphism and magmatism during the Himalayan collision, *in* Coward, M. P., and Ries, A. C., eds., Collision tectonics: Geological Society [London] Special Publication 19, p. 159–172.

Le Fort, P., 1996, Evolution of the Himalaya, *in* Yin, A., and Harrison, T. M., eds., The tectonics of Asia: New York, Cambridge University Press, p. 95–109.

Le Fort, P., Cuney, M., Deniel, C., France-Lanord, C., Sheppard, S. M. F., Upreti, B. N., and Vidal, P., 1987, Crustal generation of the Himalayan leucogranites: Tectonophysics, v. 134, p. 39–57.

Molnar, P., and England, P., 1990, Temperatures, heat flux, and frictional stress near major thrust faults: Journal of Geophysical Research, v. 95, p. 4833–4856.

Montel, J.-M., 1993, A model for monazite/melt equilibrium and application to the generation of granitic magmas: Chemical Geology, v. 110, p. 127–146.

Noble, S. R., and Searle, M. P., 1995, Age of crustal melting and leucogranite formation from U-Pb zircon and monazite dating in the western Himalaya, Zanskar, India: Geology, v. 23, p. 1135–1138.

Ohmoto, H., and Kerrick, D., 1977, Devolatilization equilibria in graphitic systems: American Journal of Science: v. 277, p. 1031–1044.

Parrish, R. R., and Hodges, K. V., 1996, Isotopic constraints on the age and provenance of the Lesser and Greater Himalayan sequences, Nepalese Himalaya: Geological Society of America Bulletin, v. 108, p. 904–911.

Patzelt, A., Li, H., Wang, J., and Appel, E., 1996, Paleomagnetism of Cretaceous to Tertiary sediments from southern Tibet: Evidence for the extent of the northern margin of India prior to the collision with Eurasia: Tectonophysics, v. 259, p. 259–284.

Pinet, C., and Jaupart, C., 1987, A thermal model for the distribution in space and time of the Himalayan granites: Earth and Planetary Science Letters, v. 84, p. 87–99.

Quidelleur, X., Grove, M., Lovera, O. M., Harrison, T. M., Yin, A., and Ryerson, F. J., 1997, The thermal evolution and slip history of the Renbu Zedong thrust, southeastern Tibet: Journal of Geophysical Research, v. 102, p. 2659–2679.

Ratschbacher, L., Frisch, W., Lui, G., and Chen, C., 1994, Distributed deformation in southern and western Tibet during and after the India-Asia collision: Journal of Geophysical Research, v. 99, p. 19817–19945.

Schärer, U., 1984, The effect of initial ^{230}Th disequilibrium on young U-Pb ages: The Makalu case, Himalaya: Earth and Planetary Science Letters, v. 67, p. 191–204.

Schärer, U., Xu, R. H., and Allègre, C. J., 1986, U-(Th)-Pb systematics and ages of Himalayan leucogranites, south Tibet: Earth and Planetary Science Letters, v. 77, p. 35–48.

Searle, M. P., Parrish, R. R., Hodges, K. V., Hurford, A. J., Ayres, M. W., and Whitehouse, M. J., 1997, Shisha Pangma leucogranite, South Tibetan Himalaya: Field relations, geochemistry, age, origin, and emplacement: Journal of Geology, v. 105, p. 295–317.

Searle, M. P., Metcalfe, R. P., Rex, A. J., and Norry, M. J., 1993, Field relations, petrogenesis and emplacement of the Bhagirathi leucogranite, Garhwal Himalaya, *in* Treloar, P. J., and Searle, M. P., eds., Himalayan tectonics: Geological Society [London] Special Publication 74, p. 429–444.

Thompson, A. B., 1982, Dehydration melting of pelitic rocks and the generation of H_2O-undersaturated granitic liquids: American Journal of Science, v. 282, p. 1567–1595.

Turcotte, D. L., and Schubert, G., 1982, Geodynamics: Applications of continuum physics to geological problems: New York, Wiley, 450 p.

Vielzeuf, D., and Holloway, J. R., 1988, Experimental determination of the fluid-absent melting relations in the pelitic system—Consequences for crustal differentiation: Contributions to Mineralogy and Petrology, v. 98, p. 257–276.

Manuscript received February 19, 1997
Revised manuscript received July 2, 1997
Manuscript accepted July 25, 1997